Atomic Engineering of Single Photon Sources in 2D Boron Nitride

Zai-Quan Xu[1, 2], Christopher Elbadawi[1], Toan Trong Tran[1], Mehran Kianinia[1], T. B. Hoffman[3], J. H. Edgar[3], Milos Toth[1, 2*], Igor Aharonovich[1, 2*]

1. School of Mathematical and Physical Sciences, Faculty of Science, University of Technology Sydney, Ultimo, 2007, New South Wales, Australia

2. Institute for Biomedical Materials & Devices (IBMD), University of Technology Sydney, Ultimo, 2007, New South Wales, Australia

3. Department of Chemical Engineering, Durland Hall, Kansas State University, Manhattan, KS 66506, USA

*Corresponding Emails: Milos.Toth@uts.edu.au; Igor.Aharonovich@uts.edu.au

Abstract

Artificial atomic systems in solids such as single photon emitters are becoming increasingly important building blocks in quantum information processing and scalable quantum nanophotonic networks. Here, we report on a controllable way to engineer emitters in two-dimensional (2D) hexagonal boron nitride (hBN) crystals using plasma processing. The method is robust, and yields a 7-fold increase in the density of emitters in hBN, which is promising for their deployment in practical devices. While as-fabricated emitters suffer from blinking and bleaching, a subsequent annealing step yields photo-stable emitters. The presented process is the first step towards controllable placement of quantum emitters in hBN for integrated on-chip quantum nanophotonics based on 2D materials.

Introduction

Two-dimensional (2D) materials such as graphene, hexagonal boron nitride (hBN) and transition metal chalcogenides are widely studied for photonics and optoelectronics due to strong light-matter interactions and layer-dependent properties.[1-5] In particular, hBN is a layered wide band gap semiconductor[6] with covalently bonded boron and nitrogen in a honeycomb structure.[7] Due to its hyperbolic properties, hBN is frequently used to enhance electronic and optical properties of other 2D materials.[8] Recently, hBN has been shown to host bright, fully polarized emitters of anti-bunched non-classical light, attributed to localized point defects in the honeycomb structure.[7, 9-11 12] To fully harness the excellent properties of these emitters and transform them into useful device components[13], a reliable method to engineer them in a crystal of choice is required. While several methods have recently been explored, including laser ablation[12], ion/electron irradiation[9] and chemical etching[14], they have so far had marginal success and extremely low yields.

Here, we demonstrate a simple, efficient and scalable approach to engineer single photon emitters (SPEs) using an argon plasma etching process followed by a high temperature annealing treatment. After etching, the quantity of the fluorescent atomic defects is 7 times higher than in as prepared samples. The emitters have zero phonon lines (ZPLs) in the visible to the near-infrared spectral ranges and their single photon nature is confirmed by measuring second order autocorrelation functions. The ability to engineer the emitters deterministically in a selected hBN crystal opens interesting pathways to integrate them in quantum nanophotonic devices.[15]

We start by demonstrating controlled fabrication of single photon emitters in a selected hBN crystal. Figure 1a shows an optical microscope image of tape-exfoliated hBN crystal on a silicon substrate. Figure 1b illustrates the plasma etching process used to fabricate the emitters. Figure 1c, d show confocal PL maps acquired at room temperature from the same crystal before and after argon plasma etching (See methods for details), respectively. Elevated photon counts outline the crystal edges and grain boundaries and the overall fluoresce intensity from the etched sample is comparable to that from the as-prepared one. Red circles show the locations of emitters found in the crystals. The majority of the emitters found before and after the plasma treatment were located at crystal edges and grain boundaries, consistent with previous studies.[9] Very few emitters were present in these hBN crystals prior to etching (Figure 1c) and they decorated bright edge site regions. On the other hand, after the plasma process the number of emitters found in the same hBN crystals increased by a factor of 3. Moreover, significantly more emitters were present in the middle of this flake, while the original emitters were located exclusively at edges. The samples were annealed in Ar at 850°C before and after the plasma treatment, as is detailed in Methods. The first annealing treatment serves as a reference to show that plasma processing is the dominant step responsible for emitter generation, while the subsequent annealing step stabilizes the emitters generated by the plasma, as is discussed below.

In addition, oxygen plasma etching was also investigated (see figure S1). The fluorescence intensity after O_2 plasma etching was higher compared to pristine hBN crystals probably due to boron oxides[16] generated during the process and more emitters were found after etching. However, the emitters exhibited severe blinking and bleaching during the measurement even after the post-plasma annealing treatment. We therefore conclude that the Ar plasma method is preferred for emitter generation.

To get a more quantitative comparison of the emitters before and after the plasma treatment, we perform a statistical analysis of the emitter ZPLs. Figure 1e shows histograms of ZPL wavelengths for emitters found in 5 different hBN crystals (area ~ 40 × 40 μm^2) that have undergone an identical plasma treatment. While only 8 emitters were found before Ar plasma etching (in all of the 5 crystals), the number of emitters increased to 66 after plasma processing. The ZPL wavelengths of the emitters are predominantly centred on ~ 600 nm, but some emitters had ZPL wavelengths longer than 750 nm. This variation in ZPL energy in hBN has been reported previously and attributed tentatively to variations in local dielectric

environment, strain and defect species.[9, 14] Figure 1f shows representative normalized spectra of emitters generated by the plasma treatment.

To explore the possibility of deterministic patterning of emitters into arrays, we employed standard photolithography to create arrays of annulus-shaped features that were processed by the 200W Ar plasma etching for 10mins. Figure 2a shows an optical microscope image of the hBN crystal. The outer diameter of each annulus is ~2 μm and the centre-to-centre distance is 4 μm. We intentionally chose a rather large flake to fit an array of ~ 9 annuli on a single crystal. After lithography, the same Ar plasma etching and annealing processes were employed. To correlate the lithographic patterns with the created emitters, confocal PL mapping was performed. Figure 2b shows a confocal image of the crystal, clearly exhibiting localized bright emitters. The red circles highlight the positions of 5 emitters found over the crystals, all of which were found to be in the vicinity of the annuli (within our confocal resolution of ~ 400 nm). Figure 2c shows PL spectra collected from these spots, demonstrating that they are narrowband emitters with ZPL energies in the range of 580 to 680 nm, consistent with the results described above. Our result put a lower limit of ~ 20% on the formation probability of the emitters in such an array. We have also employed a direct-write electron beam induced etching technique to create arrays of holes in hBN crystals[17], which were then subjected to the plasma treatment. In that case, emitters are expected to form in close proximity to the holes. The results are shown in the supporting information (figures S2, S3), and the formation probability of the emitters is also approximately 20%.

Having demonstrated the emitter fabrication process, we proceed to characterize their quantum properties. Figure 3a shows the ZPL of a representative emitter produced by the Ar plasma etch process fitted with a Lorentz function. The ZPL maximum is at ~ 712 nm and the full width at half maximum (FWHM) is ~18 nm. To evaluate the excited state lifetime, the PL decay time was measured using a 512 nm pulsed laser (Figure 3b), yielding an excited state lifetime of 2.4 ns. The inset of figure 3b shows is the second order autocorrelation function ($g^{(2)}(\tau)$) obtained from this emitter. The dip at zero delay is well below 0.5 ($g^{(2)}(0)$ ~ 0.1), confirming that the defect is a true single photon emitter. The curve was fit with a three-level model, where τ_1 and τ_2 are excited and metastable state lifetimes, respectively.

$$g^{(2)}(\tau) = 1 - a\, e^{-\tau/\tau_1} + b\, e^{-\tau/\tau_2}$$

Figure 3c depicts the fluorescence intensity as a function of excitation power. A standard three level system that has a ground, excited and a long lived metastable state was used to fit the data using the following equation,

$$I = I_{\infty} \frac{P}{P + P_{sat}}$$

where I_{∞} and P_{max} are the emission rate and the excitation power at saturation, respectively. The saturation emission rate for this emitter is 5.4×10^4 at a saturation power of 910 μW. The brightness is comparable to previous reports of emitters in tape exfoliated hBN crystals.[14] As mentioned earlier, most emitters found after the Ar plasma etching were not stable and bleach in seconds. A post-etching annealing treatment was therefore performed to stabilize the emitters. This is demonstrated in Figure 3d which compares the stability of emitters measured before and after annealing (additional stability curves are shown in Figure S4).

To study the effects of plasma etching on hBN crystals, part of an hBN crystal was protected with photo-resist to protect the flake during plasma processing, and atomic force microscopy (AFM) and Raman spectroscopy were used to compare the sample morphology and strain before and after etching. Figure 4a shows a height image of the sample surface obtained using AFM. The surface of the protected hBN remains very smooth (RMS roughness ~ 0.65 nm) which suggests it was not damaged during the etching process. By contrast, the etched area contains randomly distributed nano-islands (RMS roughness ~ 0.91 nm). Furthermore, Ar plasma etching produces a ~ 2 nm step (Figure 4b) at the etched-protected interface, suggesting that the fabricated new emitters are located in the 4 top layers of the hBN crystals. The inset of Figure 4b shows an optical image of the hBN crystal obtained after etching. Red dashed lines indicate the boundary between the etched/protected areas, and the height difference is easily observed as a change in contrast in the image.[18] The maximum penetration ranges of Ar+ and O+ ions and the corresponding vacancy generation depth profiles were simulated using the Monte Carlo code SRIM (stopping range of ions in matter).[19] The results are shown in figure 4c for an accelerating voltage of 400V (the self-biased voltage of the plasma system under the conditions used in this work). Most of the ions penetrate 2 - 3nm below the hBN crystal surface, illustrating that the plasma process is very shallow, and the emitters are fabricated within the top few nanometers of the surface. Figure 4d shows Raman spectra from the pristine and etched hBN regions of the crystal. A characteristic peak corresponding to the E_{2g} phonon mode occurs at ~1395 cm^{-1}, in etched

samples, the Raman peak is slightly shifted, typically to 1393 cm^{-1}. This shift is comparable to the one between bulk hBN and monolayers. On the other hand, the FWHMs in the etched samples is smaller than in the pristine ones.[18] The red-shifted and sharpened Raman peaks and the rougher surface on the etched flake suggest that, starting from the irregular structures at the edge/grain boundaries, the covalent bonds in hBN crystals were broken, creating smaller hBN sheets and changing the strain in the crystals.[18, 20-21]

Previously, many defects, *i.e.* anti-site vacancy, N-vacancy, B-vacancy and interlayer bonding, were proposed to be responsible for the broad range of ZPL energies in hBN.[7, 14] Argon and oxygen plasma etching were often performed on graphene and other 2D materials to prepare monolayers, and in both cases, the B-N bonds in hBN were broken and new vacancies were created.[16, 21-26] Ar plasma etching has two effects on the hBN samples, one is removal of organics on the surface of hBN crystals and the other is creation of vacancies[21], especially on grain boundary sites.[27] Hence, the generation of emitters observed here is consistent with the proposal that the underlying defect is a vacancy complex such as the antisite nitrogen vacany.[7] The fact that oxygen plasma resulted in bleaching of the emitters suggests that the defect is neutral, and excess electrons from oxygen give rise to the bleach ing.

In conclusion, we proposed a scalable technique to prepare SPEs in selected positions a non-reactive argon etch process. We showed a factor of 7 enhancement to create new emitters using the plasma technique, and showed that a subsequent annealing treatment stabilizes the emitters. AFM data indicate that the emitters are located within the top 4 layers of the hBN crystals and the emitters are likely formed preferentially at edges created during etching. Our results help to further understand the nature of point defects in hBN and pave the way to future applications of these single photon sources in quantum photonics and information processing.

Acknowledgments

The hBN crystal growth at Kansas State University was supported by NSF grant CMMI 1538127. Financial support from the Australian Research Council (via DP140102721, DE130100592), FEI Company, and the Asian Office of Aerospace Research and Development grant FA2386-15-1-4044 are gratefully acknowledged.

Methods

Sample fabrication: The hBN crystals were produced at atmospheric pressure using a molten mixture of nickel and chromium (weight ratio, 1:1) as the solvent, and isotopically enriched boron-10 metal as the boron source. The mixture was heated to and held at 1550 °C for 24 hours under flowing nitrogen. Slow (4°C/hour) cooling of this solution caused the hBN crystals to precipitate on the metal alloy surface.[28-29]

Isotopically enriched hBN (95% B10) single crystals were mechanically exfoliated with scotch tape onto a Si substrate with a 300nm thermal oxide capping layer. The crystals were annealed at 850°C in Ar for 30 min after a cleaning process comprised of a 450°C anneal in air and an oxygen plasma treatment. These "as-prepared samples" were pre-characterised, and loaded into a vacuum chamber for Ar or O_2 plasma etching using a system equipped with a 13MHz radio-frequency (RF) plasma generator. The crystals were etched with a power of 200 W under a pressure of 180 mTorr for 2 mins at room temperature. Under these conditions the ions were accelerated by a DC self-bias of ~ 400V. The crystals were subsequently annealed at 850°C in Ar for 30mins to stabilize the emitters after plasma processing.

Optical Characterization: A home-built confocal setup was used for optical characterization of the crystals. Samples were excited with a 532 nm continuous wave (CW) laser (Gem 532™, Laser Quantum Ltd.) directed through a Glan-Taylor polarizer (Thorlabs Inc.) and a half waveplate, and focused onto the sample using a high numerical aperture (NA = 0.9, Nikon) objective lens. An X-Y piezo scanning mirror (FSM-300™) was used to perform confocal scanning. The excitation laser light was blocked with a 532 nm dichroic mirror (532 nm laser BrightLine™, Semrock) and a tilted 550nm long pass filter (Semrock) at the collection end. The signal was then coupled into a graded index fiber and a fiber splitter was used to direct the light to a spectrometer (Acton SpectraPro™, Princeton Instrument Inc.) or to two avalanche photodiodes (Excelitas Technologies™) to collect spectra or autocorrelation data. Autocorrelation measurements were performed in a Hunbury Brown-Twiss configuration where the emission was equally separated and directed into two APDs. Lifetime measurements were performed using a 512 nm pulsed laser excitation source (PiL051X™, Advanced Laser Diode Systems GmbH) with a 100 ps pulse width and a 10 MHz repetition rate.

Electron beam processing: The as-prepared hBN samples were loaded into a variable pressure FEI Nova NanoSEM field emission gun scanning electron microscope. The system

was pumped down to a base pressure of $3x10^{-4}$ Pa before the chamber was filled with water vapour to a pressure of 10 Pa. The isotopically-rich hBN crystals were then located using a magnetic field assisted gas cascade detector, and irradiated using a focused electron beam (Accelerating Voltage 10 kV, Beam current 4 nA, Dwell time 0.002s). The irradiation process gives rise to defect formation and eventual etching of hBN. [17]

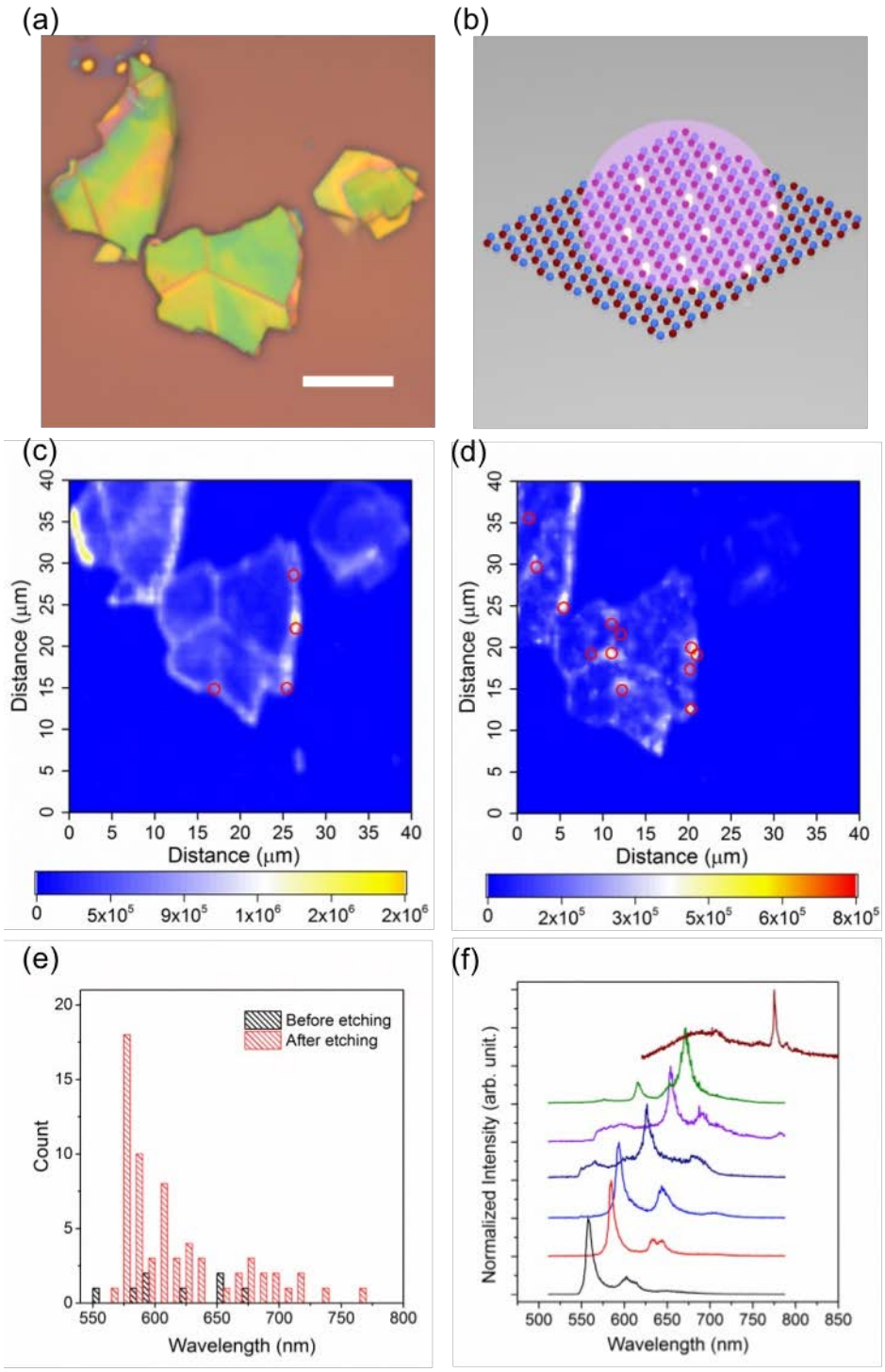

Figure 1 (a) Optical microscope image of hBN crystals. Scale bar: 10 μm. (b) Schematic image showing a hBN atomic sheet under plasma etching. (c,d) Confocal PL maps of the hBN crystals shown in (a) before and after Ar plasma etching. The red circles highlight the locations of emitters found before (c) and after (d) plasma etching. (e) Histograms of zero phonon line wavelengths of emitters found before and after plasma etching generated using a

5nm bin size. (f) Selected spectra of emitters found after plasma etching and annealing. The spectra are offset vertically for clarity.

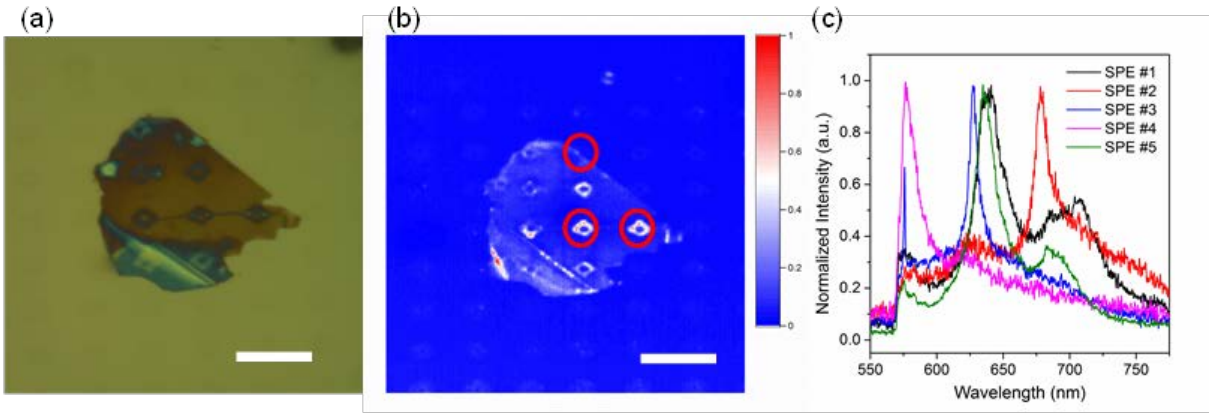

Figure 2 (a) Optical microscope image of annuli fabricated on a hBN crystal by plasma etching. Scale bar: 8 μm. (b) Normalized confocal PL map taken using a 580 nm long pass filer. (c) Selected PL spectra of emitters found in this crystal.

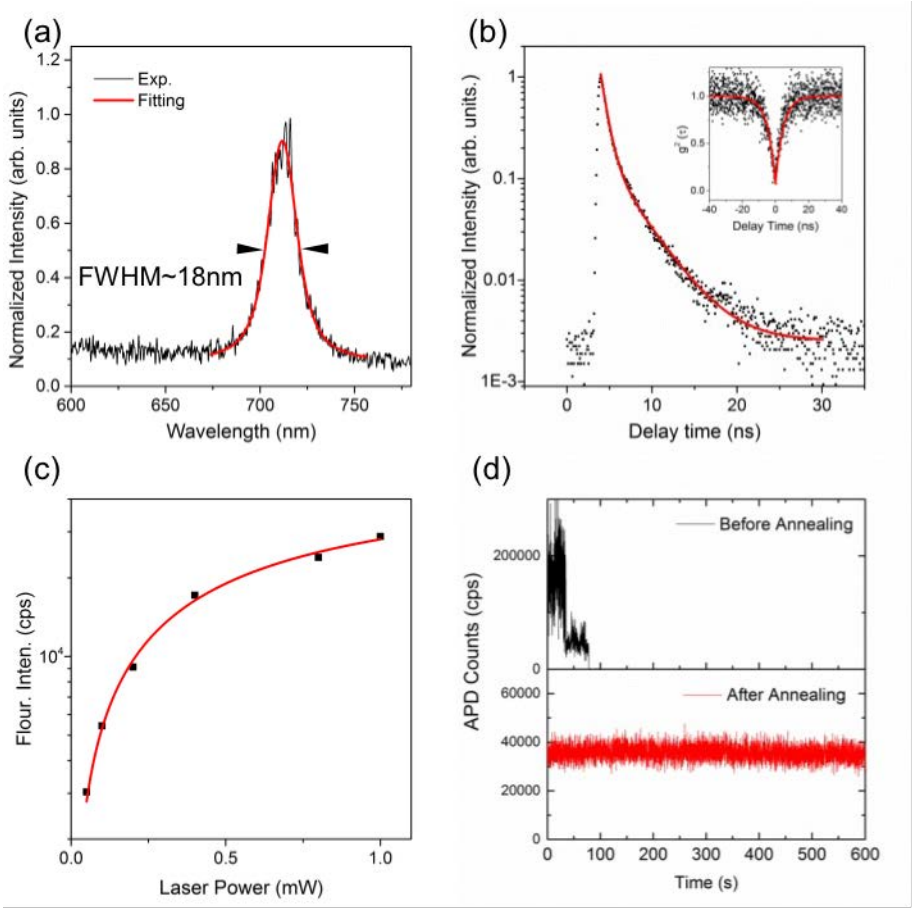

Figure 3 (a) A representative PL spectrum with an emission peak at 716 nm (fitted with a

Lorentz function) obtained from Ar plasma etched and annealed hBN crystals. (b) A time-resolved decay curve shows that the emitter lifetime is 2.4 ns. Inset: A second order autocorrelation function of the emitter fit using a three-level model with a $g^{(2)}(0) \sim 0.1$, confirming a single photon source. (c). A saturation curve of the emitter. (d) Representative emitter stability curves obtained before (black curve top panel) and after annealing (red curve bottom panel) of a plasma-etched hBN crystal.

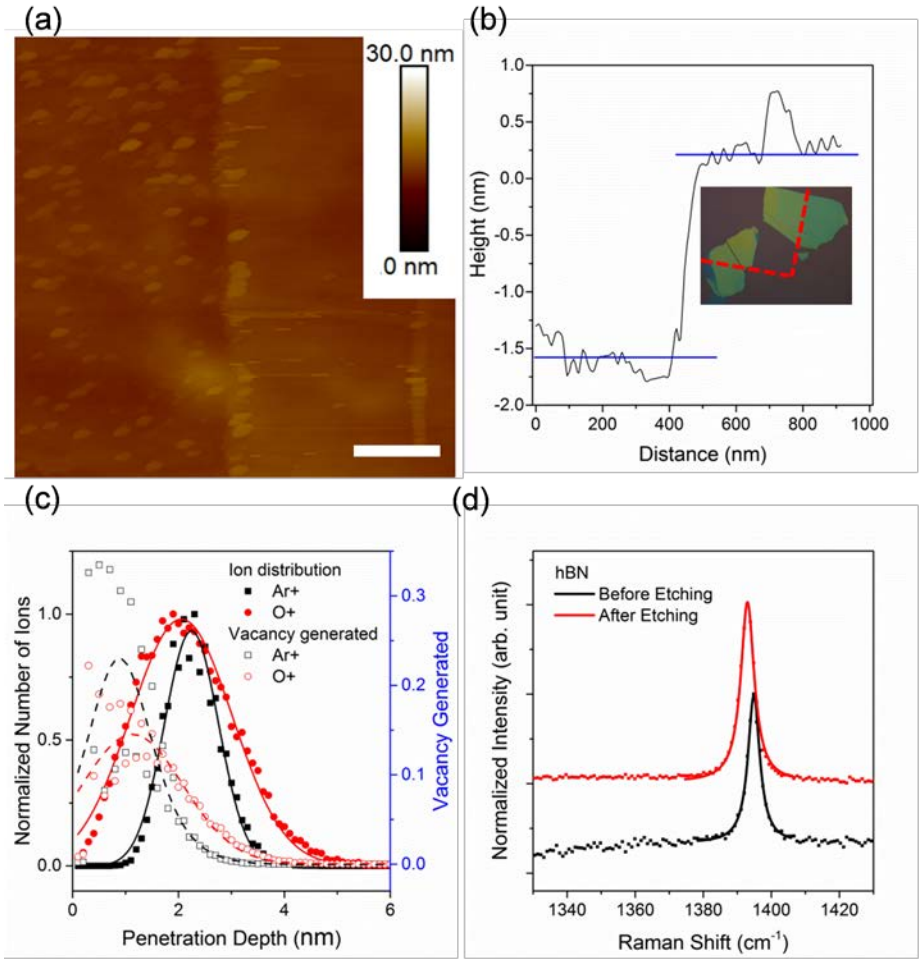

Figure 4 (a) AFM image of the interface between etched (left) and protected (right) regions of a hBN crystal. Scale bar: 1 μm (b) AFM height profile across the interface. Inset: Optical image of plasma-etched hBN crystals. The contrast seen at the dashed lines corresponds to the thickness difference produced by the etch treatment. (c) Ion depth distributions (filled squares and circles) and vacancy generation rates (hollow squares and circles) simulated for 400 eV Ar^+ and O^+ ions implanted into hBN. (d) Raman spectra obtained from pristine (black data points) and etched (red data points) regions of a hBN crystal. The spectra were offset vertically for clarity. The data were fit with Lorentizan functions.

References

1. Koppens, F. H.; Mueller, T.; Avouris, P.; Ferrari, A. C.; Vitiello, M. S.; Polini, M., Photodetectors based on graphene, other two-dimensional materials and hybrid systems. *Nature nanotechnology* **2014,** *9* (10), 780-93.
2. Ponraj, J. S.; Xu, Z. Q.; Dhanabalan, S. C.; Mu, H.; Wang, Y.; Yuan, J.; Li, P.; Thakur, S.; Ashrafi, M.; McCoubrey, K.; Zhang, Y.; Li, S.; Zhang, H.; Bao, Q., Photonics and optoelectronics of two-dimensional materials beyond graphene. *Nanotechnology* **2016,** *27* (46), 462001.
3. Baugher, B. W.; Churchill, H. O.; Yang, Y.; Jarillo-Herrero, P., Optoelectronic devices based on electrically tunable *p-n* diodes in a monolayer dichalcogenide. *Nature nanotechnology* **2014,** *9* (4), 262-7.
4. Britnell, L.; Ribeiro, R. M.; Eckmann, A.; Jalil, R.; Belle, B. D.; Mishchenko, A.; Kim, Y. J.; Gorbachev, R. V.; Georgiou, T.; Morozov, S. V.; Grigorenko, A. N.; Geim, A. K.; Casiraghi, C.; Castro Neto, A. H.; Novoselov, K. S., Strong light-matter interactions in heterostructures of atomically thin films. *Science* **2013,** *340* (6138), 1311-4.
5. Fiori, G.; Bonaccorso, F.; Iannaccone, G.; Palacios, T.; Neumaier, D.; Seabaugh, A.; Banerjee, S. K.; Colombo, L., Electronics based on two-dimensional materials. *Nature nanotechnology* **2014,** *9* (10), 768-79.
6. Watanabe, K.; Taniguchi, T.; Kanda, H., Direct-bandgap properties and evidence for ultraviolet lasing of hexagonal boron nitride single crystal. *Nature materials* **2004,** *3* (6), 404-9.
7. Tran, T. T.; Bray, K.; Ford, M. J.; Toth, M.; Aharonovich, I., Quantum emission from hexagonal boron nitride monolayers. *Nature nanotechnology* **2015,** *11* (1), 37-41.
8. Georgiou, T.; Jalil, R.; Belle, B. D., Vertical field-effect transistor based on graphene–WS2 heterostructures for flexible and transparent electronics. *Nature nanotechnology* **2012,** *8*, 100.
9. Tran, T. T.; Elbadawi, C.; Totonjian, D.; Lobo, C. J.; Grosso, G.; Moon, H.; Englund, D. R.; Ford, M. J.; Aharonovich, I.; Toth, M., Robust Multicolor Single Photon Emission from Point Defects in Hexagonal Boron Nitride. *ACS nano* **2016,** *10* (8), 7331-8.
10. Bourrellier, R.; Meuret, S.; Tararan, A.; Stephan, O.; Kociak, M.; Tizei, L. H.; Zobelli, A., Bright UV Single Photon Emission at Point Defects in h-BN. *Nano letters* **2016,** *16* (7), 4317-21.
11. Jungwirth, N. R.; Calderon, B.; Ji, Y.; Spencer, M. G.; Flatte, M. E.; Fuchs, G. D., Temperature Dependence of Wavelength Selectable Zero-Phonon Emission from Single Defects in Hexagonal Boron Nitride. *Nano letters* **2016,** *16* (10), 6052-6057.
12. Choi, S.; Tran, T. T.; Elbadawi, C.; Lobo, C.; Wang, X.; Juodkazis, S.; Seniutinas, G.; Toth, M.; Aharonovich, I., Engineering and Localization of Quantum Emitters in Large Hexagonal Boron Nitride Layers. *ACS applied materials & interfaces* **2016,** *8* (43), 29642-29648.
13. Tran, T. T.; Wang, D.; Xu, Z. Q.; Yang, A.; Toth, M.; Odom, T. W.; Aharonovich, I., Deterministic Coupling of Quantum Emitters in 2D Materials to Plasmonic Nanocavity Arrays. *Nano letters* **2017**.
14. Chejanovsky, N.; Rezai, M.; Paolucci, F.; Kim, Y.; Rendler, T.; Rouabeh, W.; Favaro de Oliveira, F.; Herlinger, P.; Denisenko, A.; Yang, S.; Gerhardt, I.; Finkler, A.; Smet, J. H.; Wrachtrup, J., Structural Attributes and Photodynamics of Visible Spectrum Quantum Emitters in Hexagonal Boron Nitride. *Nano letters* **2016,** *16* (11), 7037-7045.
15. Aharonovich, I.; Englund, D.; Toth, M., Solid-state single-photon emitters. *Nature Photonics* **2016,** *10* (10), 631-641.
16. Sevak Singh, R.; Yingjie Tay, R.; Leong Chow, W.; Hon Tsang, S.; Mallick, G.; Tong Teo, E. H., Band gap effects of hexagonal boron nitride using oxygen plasma. *Applied Physics Letters* **2014,** *104* (16), 163101.
17. Elbadawi, C.; Tran, T. T.; Kolibal, M.; Sikola, T.; Scott, J.; Cai, Q.; Li, L. H.; Taniguchi, T.; Watanabe, K.; Toth, M.; Aharonovich, I.; Lobo, C., Electron beam directed etching of hexagonal boron nitride. *Nanoscale* **2016,** *8* (36), 16182-6.

18. Gorbachev, R. V.; Riaz, I.; Nair, R. R.; Jalil, R.; Britnell, L.; Belle, B. D.; Hill, E. W.; Novoselov, K. S.; Watanabe, K.; Taniguchi, T.; Geim, A. K.; Blake, P., Hunting for monolayer boron nitride: optical and Raman signatures. *Small* **2011,** *7* (4), 465-8.
19. Ziegler, J. F., Srim-2003. *Nuclear Instruments and Methods in Physics Research Section B: Beam Interactions with Materials and Atoms* **2004,** *219-220*, 1027-1036.
20. Arenal, R.; Ferrari, A. C.; Reich, S.; Wirtz, L.; Mevellec, J. Y.; Lefrant, S.; Rubio, A.; Loiseau, A., Raman spectroscopy of single-wall boron nitride nanotubes. *Nano letters* **2006,** *6* (8), 1812-6.
21. Zeng, H.; Zhi, C.; Zhang, Z.; Wei, X.; Wang, X.; Guo, W.; Bando, Y.; Golberg, D., "White graphenes": boron nitride nanoribbons via boron nitride nanotube unwrapping. *Nano letters* **2010,** *10* (12), 5049-55.
22. Liu, Z.; Ma, L.; Shi, G.; Zhou, W.; Gong, Y.; Lei, S.; Yang, X.; Zhang, J.; Yu, J.; Hackenberg, K. P.; Babakhani, A.; Idrobo, J. C.; Vajtai, R.; Lou, J.; Ajayan, P. M., In-plane heterostructures of graphene and hexagonal boron nitride with controlled domain sizes. *Nature nanotechnology* **2013,** *8* (2), 119-24.
23. Liu, Y.; Nan, H.; Wu, X.; Pan, W.; Wang, W.; Bai, J.; Zhao, W.; Sun, L.; Wang, X.; Ni, Z., Layer-by-layer thinning of MoS_2 by plasma. *ACS nano* **2013,** *7* (5), 4202-9.
24. Huang, Y.; Wu, J.; Xu, X.; Ho, Y.; Ni, G.; Zou, Q.; Koon, G. K. W.; Zhao, W.; Castro Neto, A. H.; Eda, G.; Shen, C.; Özyilmaz, B., An innovative way of etching MoS2: Characterization and mechanistic investigation. *Nano Research* **2013,** *6* (3), 200-207.
25. Xu, Z.-Q.; Zhang, Y.; Wang, Z.; Shen, Y.; Huang, W.; Xia, X.; Yu, W.; Xue, Y.; Sun, L.; Zheng, C.; Lu, Y.; Liao, L.; Bao, Q., Atomically thin lateral p–n junction photodetector with large effective detection area. *2D Materials* **2016,** *3* (4), 041001.
26. Prado, M. C.; Jariwala, D.; Marks, T. J.; Hersam, M. C., Optimization of graphene dry etching conditions via combined microscopic and spectroscopic analysis. *Applied Physics Letters* **2013,** *102* (19), 193111.
27. Li, Q.; Zou, X.; Liu, M.; Sun, J.; Gao, Y.; Qi, Y.; Zhou, X.; Yakobson, B. I.; Zhang, Y.; Liu, Z., Grain Boundary Structures and Electronic Properties of Hexagonal Boron Nitride on Cu(111). *Nano letters* **2015,** *15* (9), 5804-10.
28. Hoffman, T. B.; Clubine, B.; Zhang, Y.; Snow, K.; Edgar, J. H., Optimization of Ni–Cr flux growth for hexagonal boron nitride single crystals. *Journal of Crystal Growth* **2014,** *393*, 114-118.
29. Kubota, Y.; Watanabe, K.; Tsuda, O.; Taniguchi, T., Hexagonal Boron Nitride Single Crystal Growth at Atmospheric Pressure Using Ni−Cr Solvent. *Chemistry of Materials* **2008,** *20* (5), 1661-1663.

Supplementary information

Atomic Engineering of Single Photon Sources in 2D Boron Nitride

Zai-Quan Xu[1, 2], Christopher Elbadawi[1], Toan Trong Tran[1], Mehran Kianinia[1], T. B. Hoffman[3], J. H. Edgar[3], Milos Toth[1, 2], Igor Aharonovich[1, 2]

1. School of Mathematical and Physical Sciences, Faculty of Science, University of Technology Sydney, Ultimo, 2007, New South Wales, Australia

2. Initiative for Biomedical Materials & Devices (IBMD), University of Technology Sydney, Ultimo, 2007, New South Wales, Australia

3. Department of Chemical Engineering, Durland Hall, Kansas State University, Manhattan, KS 66506, USA

Figure S1 (a and b) compares the confocal PL maps and the spectra collected (c and d) before and after oxygen plasma etching (in both cases, samples were annealed in Ar atmosphere). Some of the emitters show a second-order autocorrelation function (e) lower than 0.5, meaning single photon sources. But overall the emitters created were not stable. (f)

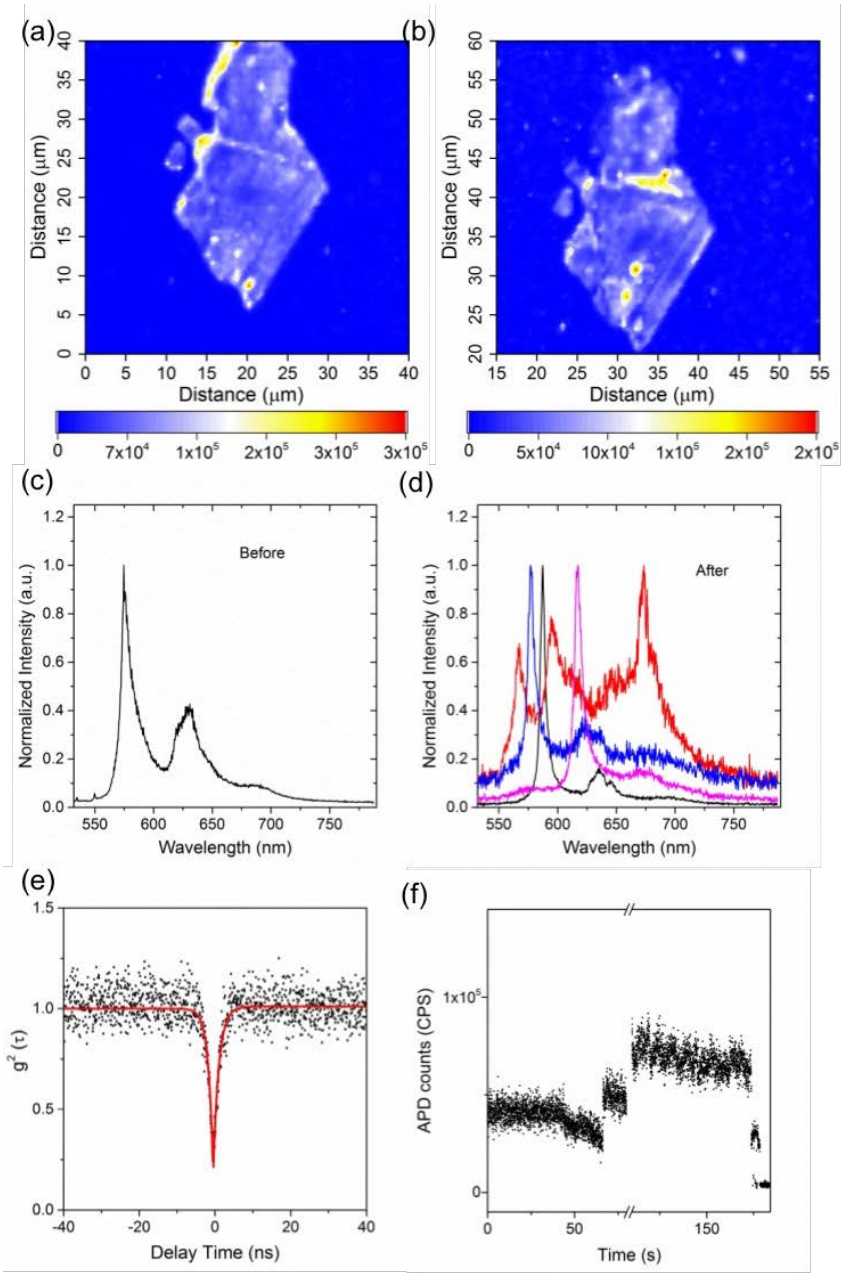

Figure S1 Confocal PL mapping over the same hBN flake before (a) and after (b) oxygen plasma etching. PL spectra of a single photon emitter found before (c) and after (d) O_2 plasma etching on the same hBN crystal. (e) Auto second correlation function of a single photon emitter created by O_2 plasma. (f) A typical APD counts as a function of time shows the poor stability of the new emitters produced from O_2 plasma.

We also explored a direct E-beam etching to define patterns into hBN to test whether new emitters were formed. Figure S3a shows the SEM image of a selected hBN crystal with the holes created by a driect ebeam writing process. The hBN flake was scanned after the holes creation, but before the plasma, and no emitters were observed. Figure 3b shows the correlated confocal mapping of the same hBN crystal after Ar plasma processing and annealing. The locations of the four new emitters were marked with green “x” signs. The formation probability in this case is ~ 4/17 circles, comparable to the ~ 20% observed also using the lithography method.

The same process was repeated with writing smaller holes. Figure S4a shows an SEM image of an hBN crystal after direct E-beam write of crosses with centre to centre distance within the cross of 1µm. Figure S4b plots the confocal PL mapping over the dash lined area shown in figure S4a. The blue circles and green “x” signs indicate the positions of the designed features and the newly formed emitters, respectively. No emitters were found on that crystals after the E-beam process but before the plasma etch. However, after plasma etching, there are 12 new emitters found in this area (figure S4c) out of the ~ 50 patterned crosses, yielding a similar formation probability of ~ 20%

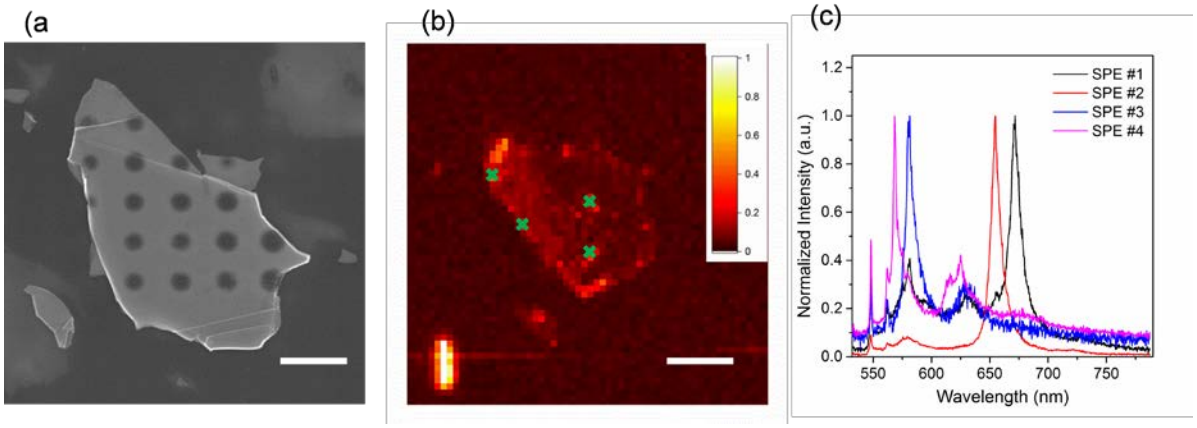

Figure S2. (a) SEM image of an hBN crystal after E-beam milling. Scale bar: 3 µm. (b) Confocal PL map of an hBN flake. The green “X” signs indicate the positions of the emitters. Scale bar: 5 µm. (c) Selective PL spectra of the emitters found at green “X” signs.

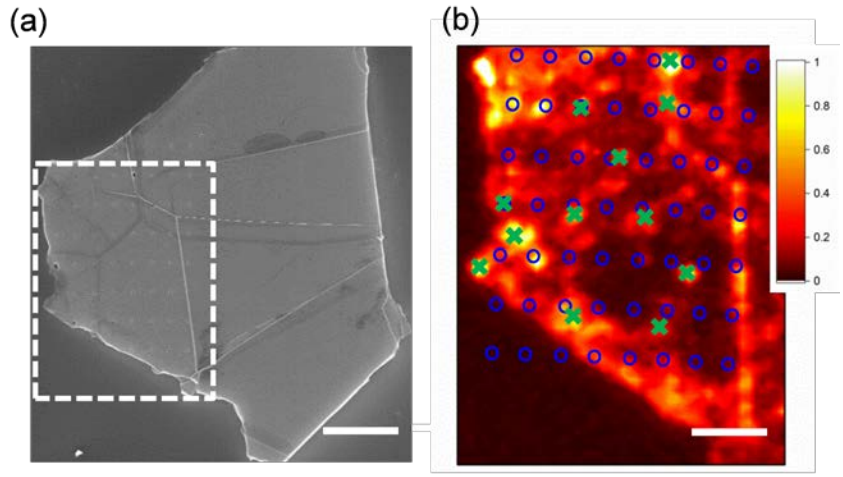

Figure S3 (a) SEM image of an hBN crystal with a periodic array of crosses etched onto the surface using an electron beam. Scale bar: 4 μm. (b) Confocal PL map of the hBN flake outlined with white dash line in (a). The blue circles and green "X" signs indicate the positions of the etch pits and emitters, respectively. Scale bar: 4 μm.

Figure S4 shows examples of the stability curves of the emitters that formed after plasma processing and undergone the 2nd annealing step.

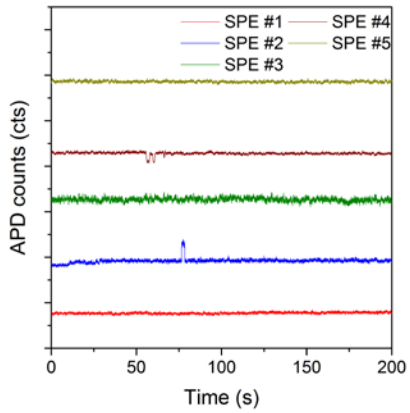

Figure S4 Stability curves from four different emitters found in hBN crystals after plasma and annealing.